Journal of Fluids and Structures (2000) **14,** 25–48
doi:10.1006/jfls1999.0233, available online at http://www.idealibrary.com on IDEAL®

SELF-SUSTAINED OSCILLATION INDUCED BY HORIZONTAL COVER PLATE ABOVE CAVITY

C.-H. Kuo, S.-H. Huang and C.-W. Chang

Department of Mechanical Engineering, National Chung-Hsing University, Taichung 40227, Taiwan, R.O.C.

(Received 15 December 1998 and in revised form 19 May 1999)

When a horizontal cover plate is placed above a cavity, the mechanism leading to enhanced self-sustained oscillation within the cavity is investigated by experiment at a Reynolds number $\mathrm{Re}_{\theta_o} = 171 \pm 5$. As the leading edge of the cover plate is located right above the most sensitive region of the cavity shear layer, the oscillating amplitude of shear layer instability is enhanced most effectively. However, this effectiveness decreases when the leading edge of the cover plate moves further downstream of the cavity. Three mechanisms are found to possibly modify the shear layer instability across the cavity. First of all, insertion of a horizontal cover plate above the cavity does impose a favourable streamwise pressure gradient that accelerates the flow across the cavity. This flow acceleration increases the amplification rate of shear layer instability. Second, the boundary layer characteristics (both the frequency band and the fluctuating amplitude) may also provide another opportunity to perturb the shear layer instability. Third, the shear layer is deflected into the cavity and leads to strong feedback. In the present study, all three mechanisms are equally important when the leading edge of the cover plate is positioned above the cavity mouth. However, when the leading edge of the cover plate is located downstream of the cavity, the first and the second effects diminish. In this situation, the stronger feedback due to the inward-deflected shear layer (the third effect) plays an important role to modify the shear layer instability.

1. INTRODUCTION

As discussed in the review paper of Rockwell & Naudascher (1978), cavity flows for various engineering applications had been the subject of endeavored research during the past decades. In high-speed applications, flow over the aircraft weapon bays, wheel wells and other airframe cutouts will produce acute noise and serious buffeting (Heller & Bliss 1975). On the other hand, hydraulic gate slots, pipes of bellow-type geometry and the heat transport phenomena over electronic devices on printed circuit boards (Ghaddar *et al.* 1986) are important low-speed applications. The separated shear layer across the cavity is liable to be subject to self-sustained oscillations if certain conditions are satisfied (Rockwell & Naudascher 1978; Blake 1980). As a result of self-sustained oscillation, perpetually large pressure fluctuations can produce fatigue damage to the components around or inside the cavity (Ethembabaoglu 1973). Moreover, high-intensity noise (Franke & Carr 1975) and significant increase of cavity drag (Gharib & Roshko 1987) are other results of the self-sustained oscillation. In an attempt to solve these undesirable problems, insightful understanding and control of the self-sustained oscillation within the cavity are of central importance.

Initiation and preferred modes of the self-sustained oscillation depend strongly upon several important factors: the turbulence level (Miskad 1972; Zaman & Hussain 1980), the

0889–9746/00/010025 + 24 $35.00/0

magnitude of incoming velocity (Heller & Bliss 1975; Knisely & Rockwell 1982), the flow conditions (either a laminar or turbulent boundary layer) at the upstream edge of the cavity (DeMetz & Farabee 1977) and the width to depth ratio (Knisely & Rockwell 1982; Gharib 1987). Other studies related to cavity can be found in Pereira & Sousa (1995) and in Ghaddar *et al.* (1986). In addition, the theoretical analysis of Michalke (1972) showed that the Strouhal number decreased monotonously from the Blasius profile to the hyperbolic tangent velocity profile (or abbreviated as tanh-velocity profile hereafter).

Unlike the free shear layer, the self-sustained oscillation of the cavity shear layer tends to be much more coherent. The coherent oscillation is caused by the feedback condition reflected from the downstream surface upon which the shear layer impinges. The selective amplification characteristic of the shear layer instability within the cavity and the upstream propagating feedback provide a necessary condition for the oscillations to be self-sustaining (Rockwell & Naudascher 1978). Furthermore, the amplitude of the self-sustained oscillation depends strongly upon the vertical offset at the downstream edge of the cavity (Rockwell & Knisely 1979). For example, as the downstream edge is modified to be a ramp instead of a step, the amplitude of fluctuating pressure inside the cavity (Ethembabaoglu 1973) and the aero-acoustic noise can be effectively reduced (Franke & Carr 1975). On the control aspect, external excitation at frequencies within the selective frequency range of shear layer instability can promote the oscillating amplitude within the cavity (Gharib 1987) if the perturbation level exceeds the threshold value. More recently, Vakili *et al.* (1993) found that the control effectiveness of the cavity oscillation depends strongly upon the upstream mass injection patterns.

In the lower reservoir of pumped-storage hydroelectric power plants, the pier structure in the vicinity of the gate slot directs the flow into the downstream diffuser with relatively small divergence angle, and thus minimizes the head loss. Although the self-sustained oscillation across the cavity in uniform flow has been investigated intensively in the past, fatigue damage occurred on the wall surface of the gate slot and on the surrounding components in the presence of a pier structure, the mechanism for which is still not completely understood. This gives the motivation of the present study: to investigate the influence of a horizontal cover plate (or the pier structure) on the evolution of the cavity shear layer. As the first approach to this problem, the Froude number will be excluded. Therefore, in this study, only the simplified two-dimensional rectangular cavity model (gate slot) is investigated when a horizontal cover plate (pier structure) is positioned above the cavity.

2. EXPERIMENTAL SET-UP

2.1. Specifications of Model and Coordinate System

As shown in Figure 1(a, b), the cavity model is two-dimensional and rectangular in geometry, and is located downstream of the contraction section. The width to depth ratio of the cavity is $L/D = 2$ with $D = 2{\cdot}5$ cm. The aspect ratio of the cavity model is $S/D = 16$. The contraction profile (1·5 m in length) is approximated by a fifth-order polynomial and continuously merges into a horizontal part (about 5 cm long), located immediately upstream of the cavity. This profile is precisely machined by a CNC mill and carefully polished to minimize the influence of surface roughness on the boundary-layer structure, especially at the upstream edge of the cavity. It is intended to maintain a more uniform inflow condition and an attached boundary-layer flow before reaching the cavity. The whole model rests on a full-span two-dimensional horizontal platform placed 5 cm above the bottom of the water channel. The flow rate between the platform and the channel bottom can be carefully

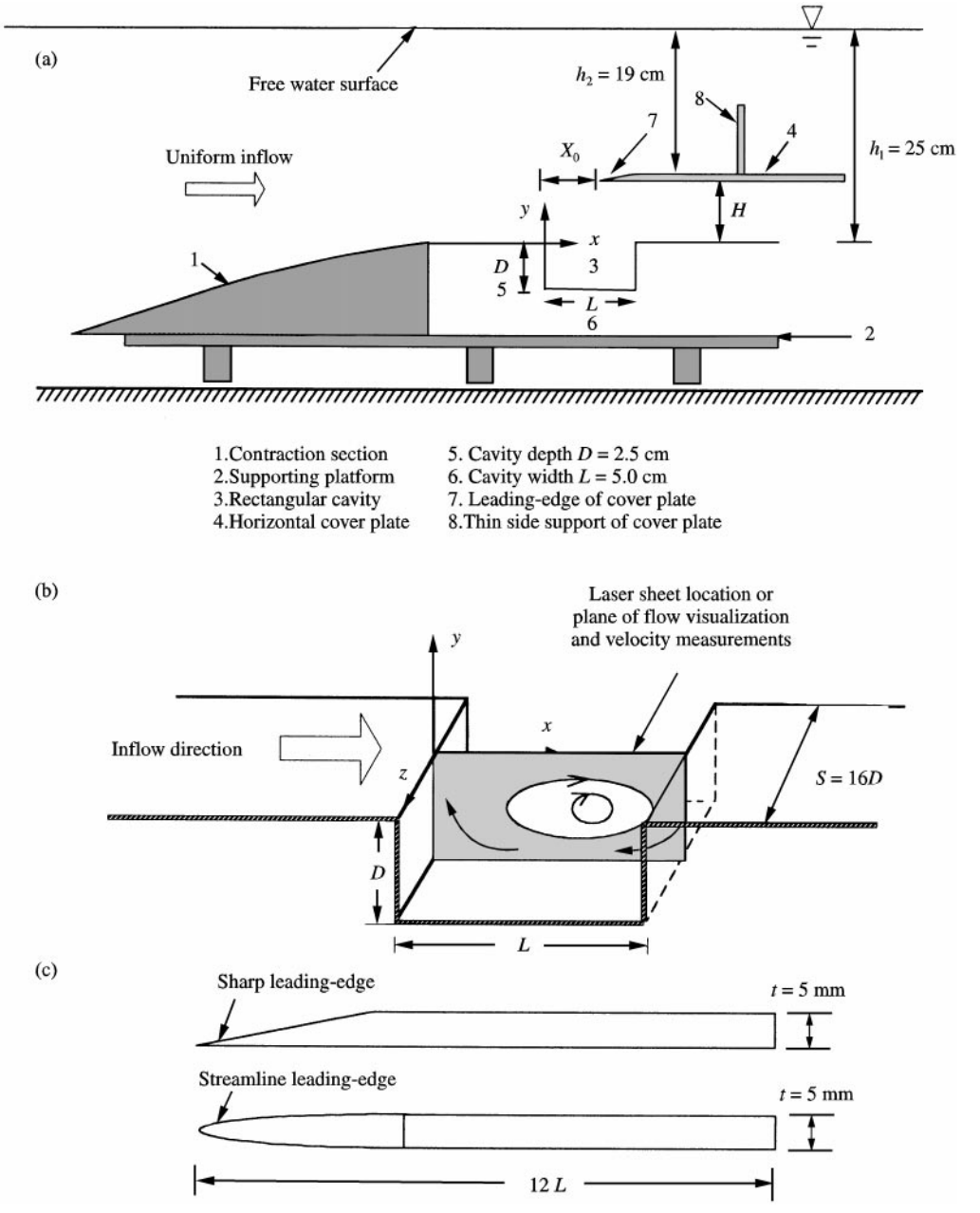

Figure 1. Experimental set-up showing (a) the specifications of the cavity model and the horizontal cover plate above the cavity, (b) the coordinate system and the plane of flow visualization and velocity measurement, and (c) the thin cover plate with sharp and streamlined leading edge.

regulated by a properly tuned steady two-dimensional suction. This allows the uniform inflow to have zero incident angle relative to the leading edge of the contraction. A horizontal cover plate (5 mm thick), parallel to the inflow direction, is placed at a fixed height ($H/D = 2{\cdot}4$) above the cavity. As shown in Figure 1(c), the leading-edge profiles of the cover plate in this study are in the form of either an upward-beveled two-dimensional sharp or a streamlined leading edge.

As depicted in Figure 1(a, b), the origin of the coordinate system is defined at the upstream edge of the cavity ($x = 0$ and $y = 0$). The positive x and y denote the directions along and upward normal to the incoming flow, respectively. Moreover, in Figure 1(c), $z = 0$ defines the plane at the mid-span where the flow visualization and intensive velocity measurements are performed. Here X_0/L represents the nondimensional streamwise distance of the leading edge of the cover plate from the origin. Also, H/D denotes the nondimensional vertical height of the cover plate above the cavity. The value $H/D = 2{\cdot}4$ is selected to prevent the free water surface from rippling. Furthermore, the horizontal cover plate is long enough (about 60 cm or $12L$) to minimize the perturbation, induced by the periodic vortex shedding from the trailing end of the cover plate.

In Figure 1(b), the self-sustaining oscillatory flow pattern is illuminated by a laser sheet cast on the flow visualization plane at mid-span (namely, $z = 0$). The fluorescent dye is fed by gravity through a constant but low-head reservoir that properly controls the flow rate of the dye. In this way, the fluorescent dye can be released naturally and steadily from a tiny hole of 0·5 mm situated about $15\theta_0$ upstream of the origin (namely, the upstream edge of the cavity), where θ_0 is the boundary layer momentum thickness at the upstream edge of the cavity.

2.2. Flow Conditions

All experiments were performed in a recirculating water channel. The test-section has a 40×40 cm square cross-section and is 300 cm long. At the upstream edge (or $x = 0$), the mean streamwise velocity profiles $\bar{u}(y)$ are measured at ten spanwise locations. The distance between two adjacent spanwise locations is $\Delta z/S = 0{\cdot}1$ apart. All the measured $\bar{u}(y)$ profiles maintain nearly the same within 96·3% of the whole span and have maximum variation about 0·86%. The boundary layer thickness from the sidewall is 1·875% of S at $x = 0$ cm and $y = 1$ cm (above the upstream edge), and 2·31% of S at $x = 5{\cdot}0$ cm and $y = 1$ cm (above the downstream edge), respectively; S represents the whole span of the test section. This implies that the secondary swirling flow, formed in the corner of the accelerating ramp and the side wall, will have only insignificant effect on the shear layer structure across the cavity mouth. Near the upstream edge ($x = 0$ and $y = 0$) of the cavity, a hydrogen-bubble wire is placed along the spanwise direction to qualitatively visualize the top-view flow structure across the cavity. In the case of no cover plate, the top-view flow structure can be observed as a flat and smooth surface grazed across the cavity up to $x/L = 0{\cdot}8$ (namely, a quasi-two-dimensional laminar flow). When the cover plate is positioned above the cavity, three-dimensional small-scale structures are observed downstream of $x/L = 0{\cdot}6$. However, the principal flow structure still maintains quasi-two-dimensional in nature.

Insertion of a horizontal cover plate above the cavity certainly gives rise to a blockage effect. However, for all the experiments studied herein, the uniform incoming velocity at $x/L = -0{\cdot}5$ is kept at the same flow speed (20 cm/s), and the shape factor at the upstream edge of the cavity varies in the range $\delta_0^*/\theta_0 = 2{\cdot}28$–$2{\cdot}52 \pm 0{\cdot}12$. Usually, for a cavity in uniform flow, the Reynolds number is defined as $\mathrm{Re}_{\theta_0} = U_\infty \theta_0/\nu$. Here U_∞ is the uniform inflow velocity and θ_0 is the momentum thickness measured at the upstream edge of the cavity. In the case that the cover plate is positioned above the cavity, the flow between the cover plate and the cavity is accelerating (refer to Section 3.2 for details). Therefore, it is proper that the Reynolds number be defined as $\mathrm{Re}_{\theta_0} = (U_0)_\infty \theta_0/\nu$. In this definition, the uniform incoming velocity U_∞ is replaced by $(U_0)_\infty$ that represents the velocity outside the boundary layer measured at $x = 0$. In the present study, this Reynolds number is kept around 171 ± 5. Likewise, the Strouhal number $\mathrm{St}_L = f_0 L/(U_0)_\infty$ is evaluated based upon the same characteristic velocity $(U_0)_\infty$. What is more, the free water surface is maintained at 25 cm (or 312 θ_0) above the cavity and 19 cm (or 235) above the cover plate.

The velocity spectra, measured in the free stream at various streamwise locations and across the height of the test section, show only wide band characteristics at the noise level, without any spectral peak. This preliminary test further ensures no detectable oscillation induced by the free water surface when the speed is maintained at 20 cm/s. At a streamwise location $30\theta_0$ upstream of the cavity, the turbulence intensity in the uniform incoming stream is 0·42%.

2.3. Velocity Measurement and Data Acquisition

For all the flow conditions studied herein, velocity measurements of $\bar{u}(y)$ along the spanwise direction and qualitative top-view flow visualization by the hydrogen-bubble technique ensure a quasi-two-dimensional flow structure across the cavity mouth. Therefore, detailed velocity measurements are performed only on the mid-span plane (at $z = 0$) by a one-component laser Doppler velocimetry system, operated in the backscatter mode. This system consists of a laser source, a Bragg cell for frequency shifting, an integrated receiving module and a correlation-based signal analyzer. It is the advantage of this nonintrusive technique that no probe interference is introduced during the measurements, especially within the most sensitive region of the cavity shear layer. Within the flow field, a precise traversing table of 0·01-mm accuracy controls the position of each measuring location. Besides, small size of the seeding particle (TiO_2, 8 μm in averaged diameter) in the water flow is required to give a response time of around 6·2 μs. Relative to the time scale in the water flow, the sufficiently fast responding time of the seeding particles ensures that the particle motion will follow naturally the fluid motion. Furthermore, proper seeding concentration in the water will produce a continuous time signal for the velocity measurement by the laser Doppler velocimetry system.

All the velocity time signals are fed into a low-pass filter whose bandwidth is set to be 80 Hz to avoid aliasing. Then, the velocity signals are digitized by a 12-bit A/D converter whose maximum sampling rate is 330 kHz. For the mean velocity measurements, a long sampling period, including 80 s (or 250 cycles), indeed provides statistically invariable averaged values. The measurement uncertainty of the uniform incoming velocity (20 cm/s) was estimated to be about 0·42%. For the oscillatory flow within the cavity, the central frequency of interest (f_0) varies around 3·6–4·0 Hz and the maximum uncertainty of the peak frequency is around 0·3%. The sampling frequency of 100 Hz and the sampling period of 20·48 s (or 80 cycles) give rise to a frequency resolution of 0·048 Hz and cut-off frequency of 50 Hz. At each measuring location, an average of 10 sample power spectral density (PSD) distributions yields the ensemble-averaged PSD. The root-mean-squared (r.m.s.) amplitudes of self-sustaining oscillation are extracted from the background noise using a bandwidth of 0·5 Hz about the central frequency (3·6–4·0 Hz). The maximum r.m.s. amplitude of $\tilde{u}(y)$ at each x/L location occurs at an elevation where the local velocity reaches 90% of U_{max}. This elevation is located approximately around $y = 0$–2 mm (or on the high-speed side of the cavity shear layer). Note that the elevation $y = 0$ represents the horizontal line that connects the upstream and the downstream edges of the cavity.

3. RESULTS AND DISCUSSION

3.1. Qualitative Flow Patterns

Figure 2(a) shows a snapshot of the flow pattern across the cavity without a cover plate. Figure 2(b–d) shows snapshots of the oscillatory flow patterns when the cover plate with a sharp leading edge is positioned at various X_0/L locations above the cavity. The

downward arrow on each photo denotes the location of the upstream edge where the separated shear layer initiates. Without the cover plate [Figure 2(a)], the separated shear layer does not exhibit any oscillating behaviour within $0 < x/L < 0{\cdot}6$ but shows a very small wavy amplitude near $x/L = 0{\cdot}8$–$1{\cdot}0$. Under this situation, a quasi-steady large-scale recirculation pattern is observed as the dominant flow structure inside the cavity. The small oscillating amplitude of the shear layer near $x/L = 0{\cdot}8$–$1{\cdot}0$ clearly indicates the onset stage of oscillation.

However, in Figure 2(b), the shear layer structure across the cavity changes remarkably when the leading edge of the cover plate is located at $X_0/L = 0$ and $H/D = 2{\cdot}4$. In this figure, the shear layer forms a small crest near $x/L = 0{\cdot}2$–$0{\cdot}3$ indicating the onset of shear layer instability. Subsequently, it rolls up into a matured vortex structure near the downstream edge ($x/L = 0{\cdot}9$) with a wavelength $\lambda \approx L/2$. The matured vortex structure will be deformed at $x/L = 1{\cdot}0$ as a result of impingement on the downstream edge. Near $x/L = 1{\cdot}0$, the deformed vortex may experience clipping in a complete or a partial form. Sometimes, it will escape from being clipped into the cavity. The snapshot in Figure 2(b) represents an example of partial escape (PE) interaction with the downstream edge.

When compared with Figure 2(a), the oscillating amplitude in Figure 2(b) is significantly enhanced and the wavelength of the shear layer instability is well defined. However, in Figure 2(c, d), the wavy flow patterns clearly indicate the reduction of oscillating amplitude when the leading edge of the cover plate moves to $X_0/L = 1{\cdot}0$ and $X_0/L = 2{\cdot}0$ locations at the same height ($H/D = 2{\cdot}4$). When the leading edge is located at $X_0/L = 3{\cdot}0$ (not shown here), the oscillation pattern closely resembles the onset oscillation in Figure 2(a). Careful examination of the shear layer structures in Figure 2(a–d) further reveals that the wavelengths of the self-sustained oscillation are nearly the same ($\lambda \approx L/2$), but there are distinct differences in the oscillating amplitudes. Similar flow characteristics can also be found for the streamlined leading-edge profile located from $X_0/L = 0$ to $2{\cdot}0$. However, the oscillating amplitudes are smaller than those for the sharp leading-edge profile.

Cavity flows are known to exhibit a "jitter" phenomenon which is attributed to possible nonlinear interaction of the cavity shear layer, either by forcing due to the shedding of the recirculation region (Pereira & Sousa 1995) or by feedback as a result of impingement on the downstream edge. For example, various possible vortex and downstream edge interactions will lead to noticeable amplitude modulation (Rockwell & Knisely 1979) and is one of the reasons to cause the jitter phenomenon in cavity flows. In the present study, the jitter phenomenon within the cavity can also be observed during long-time flow visualization. However, there is no evidence that shows the existence of a subharmonic component within the cavity (Knisely & Rockwell 1982). The details of the shear layer (or vortex) and downstream edge interaction are discussed in Section 3.7.

3.2. Outer Mean Flow Across Cavity

Typical mean streamwise velocity profiles $\bar{u}(y)$ are depicted in Figure 3 for the case when the cover plate is positioned above the cavity. At each x/L location, the magnitude of $\bar{u}(y)$ approaches to a local maximum U_{max}. The $\bar{u}(y)$ distribution maintains uniformity at large y above the cavity and outside the boundary layer of the cover plate. Besides, the magnitude of U_{max} increases from U_∞ across the cavity mouth and is a function of x/L. In Figure 4, streamwise variations of the nondimensional velocity, $u^* = U_{max}(x)/U_\infty$, measured along $y = H/2$ are plotted as functions of x/L when the leading edge of the cover plate is situated at different X_0/L locations and fixed height. Note that the vertical arrows in Figure 4 indicate the various leading-edge locations of the cover plate.

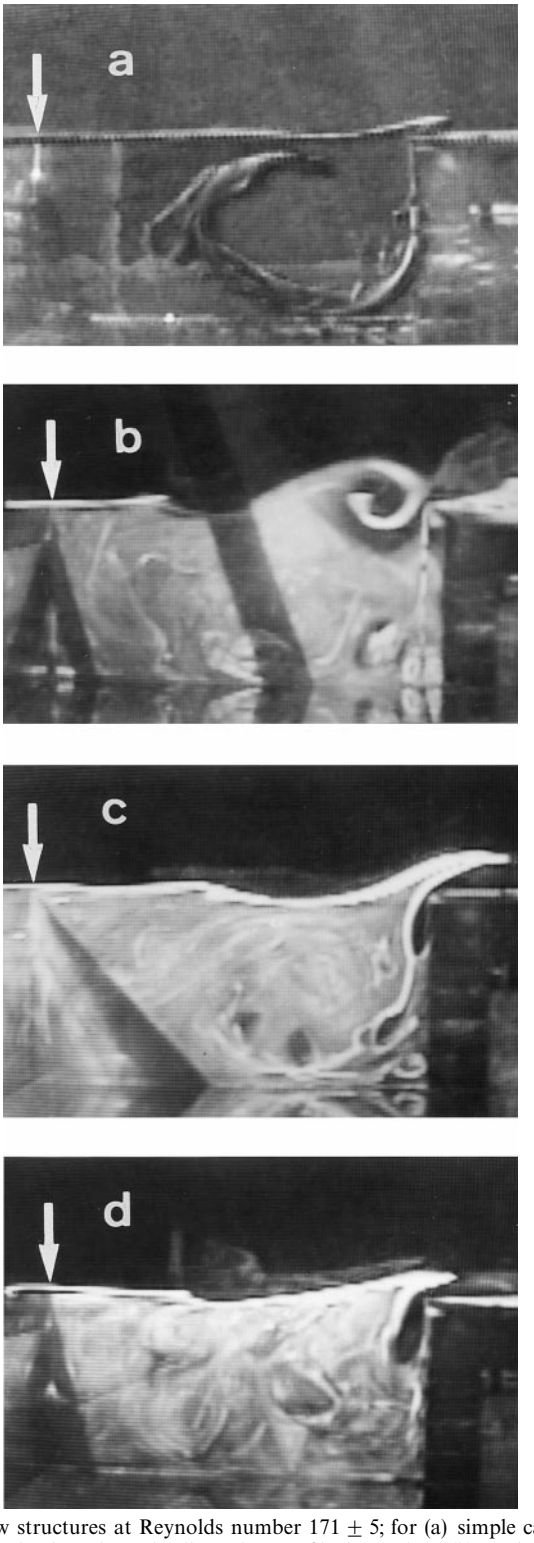

Figure 2. Oscillatory flow structures at Reynolds number 171 $\pm$ 5; for (a) simple cavity without cover plate, and (b, c, d) for cover plate having sharp leading-edge profile located at (b) $X_0/L = 0$, (c) $X_0/L = 1{\cdot}0$ and (d) $X_0/L = 2{\cdot}0$. The height is kept at $H/D = 2{\cdot}4$ for all these cases.

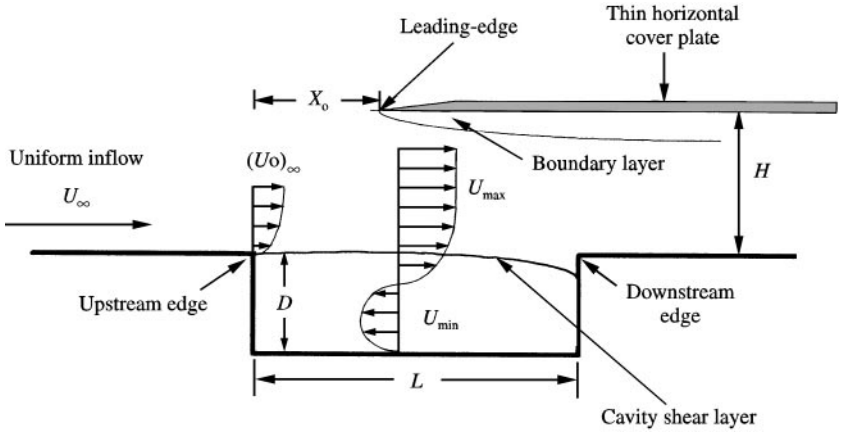

Figure 3. Typical mean streamwise velocity profiles $\bar{u}(y)$ between the cover plate and the cavity. The detailed boundary-layer structures adjacent to the cover plate for different leading-edge profiles are shown in Figure 10.

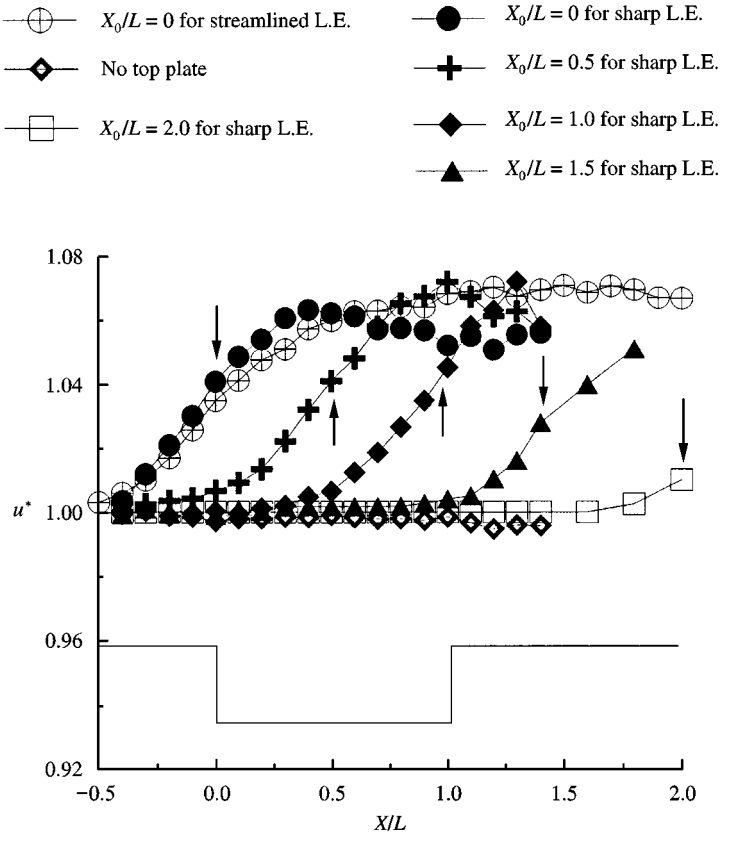

Figure 4. Streamwise variation of the u^* across the cavity mouth for leading-edge locations (marked by the arrows) of the cover plate from $X_0/L = 0$ to 2·0 and at $H/D = 2{\cdot}4$. The streamlined and sharp leading-edge profiles are compared for the $X_0/L = 0$ case. All the u^* are measured along $y = H/2$ across the cavity mouth.

For cavity flow without a cover plate, the magnitude of u^* remains nearly constant, which implies a negligible streamwise pressure gradient across the cavity mouth. As the leading edge of the cover plate is positioned above the cavity at various locations ($X_0/L = 0$–$2{\cdot}0$), the inflow speed still remains unchanged within the region farther upstream of the leading-edge locations (i.e., the vertical arrows) of the cover plate. Flow acceleration begins from $31\theta_0$ to $45\theta_0$ upstream of the leading-edge locations. Subsequently, the flow takes nearly constant acceleration (or constant slope) until u^* reaches a maximum value. During the acceleration stage, all the magnitudes of u^* increase by nearly the same amount of 7% of U_∞. Maximum deviation among these measurements is around 0.42% of U_∞. Here U_∞ denotes the uniform incoming velocity measured at $x/L = -0{\cdot}5$. After the acceleration stage, the magnitudes of u^* maintain nearly constant values except for the cases $X_0/L = 0$ and $0{\cdot}5$. In these two cases, the deviation from a constant value of u^* is caused by larger oscillating amplitude or by a matured vortex in Figure 2(b) across the cavity. As shown in Figure 4, when the cover plate is positioned at a fixed height above the cavity, the magnitudes of flow acceleration are nearly independent of the leading-edge profiles and the leading-edge locations (X_0/L) of the cover plate. However, the flow acceleration region depends strongly on the leading-edge locations.

A remarkable finding is that when the leading edge of the cover plate is positioned at $X_0/L = 0$, the most sensitive region (or $x = 0$) of the cavity shear layer undergoes a significant flow acceleration. However, the most sensitive region of the shear layer is situated within a region of mild flow acceleration when the leading edge of the cover plate moves to $X_0/L = 0{\cdot}5$. In the case $X_0/L = 2{\cdot}0$, the flow acceleration occurs downstream of the cavity and the acceleration effect becomes negligible across the cavity. However, the flow speeds near the downstream edge for the case of $X_0/L = 2{\cdot}0$ are still slightly higher than that without a cover plate. The larger the flow acceleration near $x = 0$, the thinner the momentum thickness θ_0 (Table 1). Thus, a higher growth (or amplification) rate of the shear layer instability will be expected.

3.3. Mean Flow across Shear Layer

As depicted in Figure 3, the $\bar{u}(y)$ profile will reach a local maximum value and maintain uniform distribution at locations well above the cavity and outside the boundary layer of the cover plate. The velocity profiles $\bar{u}(y)$ will encounter a very strong velocity gradient

Table 1

Momentum thickness θ_0 is measured at $x = 0$. The Strouhal number St_{θ_0} corresponds to the most unstable mode of the cavity shear layer instability for various X_0/L locations at $H/D = 2{\cdot}4$. The Reynolds numbers is 171 ± 5. The uniform incoming velocity is maintained at 20 cm/s. The maximum deviation of θ_0 is 0·42%. The maximum deviation of St_{θ_0} is around 2·0%. The units for θ_0 are mm

	No cover plate	$X_0/L = 0$	$X_0/L = 0{\cdot}5$	$X_0/L = 1{\cdot}0$	$X_0/L = 1{\cdot}5$	$X_0/L = 2{\cdot}0$
Cover plate with sharp leading-edge profile						
θ_0	0·878	0·746	0·813	0·817	0·822	0·831
St_{θ_0}	0·0157	0·0134	0·0140	0·0142	0·0145	0·0145
Cover plate with streamlined leading-edge profile						
θ_0	0·878	0·764	0·823	0·843	0·849	0·859
St_{θ_0}	0·0157	0·0132	0·0145	0·0148	0·0152	0·0154

$(\partial\bar{u}/\partial y)$ across the shear layer. Furthermore, the magnitude of $\bar{u}(y)$ will reach a local minimum $U_{\min}$ as y moves continuously into the cavity. In the present study, the velocity profiles measured at $x/L = 0{\cdot}5$ are nondimensionalized to compare with the theoretical tanh-velocity profile. In Figure 5(a), the nondimensional velocity is defined as $U^* = (\bar{u} - U_{\min})/(U_{\max} - U_{\min})$ and $y^+ = (y - y_{1/2})/\theta(x)$. Here $y_{1/2}$ represents the local elevation where U^* equals 1/2. The local momentum thickness $\theta(x)$ of the shear layer is defined as

$$\theta(x) = \frac{1}{(U_{\max} - U_{\min})^2} \int_a^b (U_{\max} - \bar{u})\,(\bar{u} - U_{\min})\,\mathrm{d}y. \tag{1}$$

In equation (1), the lower and the upper limits of the integral, a and b, correspond to the transverse locations of the local minimum and maximum velocities.

When the leading edge is placed at various X_0/L locations and $H/D = 2{\cdot}4$, Figure 5(a) shows that all the distributions of $U^*(y^+)$ collapse onto the theoretical tanh-velocity profile (Michalke 1972). The maximum deviation is around 3·2% from the theoretical curve. Furthermore, all the nondimensional mean streamwise velocity profiles, measured at successive x/L locations across the cavity, clearly show the self-similar profiles across the cavity mouth (Chang 1996). These results strongly suggest the linear growth of the momentum thickness across the cavity (Gharib & Roshko 1987). Similar characteristics of $U^*(y^+)$ can also be found for the streamlined leading-edge profile (Huang 1998).

Streamwise distributions of the local momentum thickness $\theta(x)$ of the shear layer across the cavity are illustrated in Figure 5(b) for all flow conditions in the present study. Both coordinates are normalized by the individual momentum thickness θ_0 for each flow condition. In this plot, all the streamwise variations of the local momentum thickness increase almost linearly across the cavity, except the case $X_0/L = 0{\cdot}5$. The slope is the greatest when the leading edge is located at $X_0/L = 0$. However, the slopes become much smaller (marked as the hatched region) when the leading-edge position of the cover plate moves downstream in the region $X_0/L \geq 1$. Even in the case $X_0/L = 2{\cdot}0$, the slope of $\theta(x)/\theta_0$ is still slightly higher than that without a cover plate.

As the leading edge is positioned at $X_0/L = 0$, the largest slope of the streamwise distribution of $\theta(x)/\theta_0$ is mainly caused by the strongest flow acceleration near the origin $x = 0$ (refer to Figure 4) and two other mechanisms (refer to Section 3.8). In the case $X_0/L = 0{\cdot}5$, however, there appears two distinct slopes with $x/\theta_0 \approx 27$ as a dividing point. Within the region $x/\theta_0 \leq 27$, the smaller slope implies the slow growing of $\theta(x)/\theta_0$. In this region, the flow acceleration near the origin ($x = 0$) becomes mild. Thus, the smaller slope is caused primarily by two other mechanisms. Whereas, in the region $x/\theta_0 > 27$, the slope increases and approximately equals that of $X_0/L = 0$ because stronger flow acceleration and two other effects (Section 3.8) are equally important downstream of $x/\theta_0 \approx 27$. The underlying flow physics and the mechanisms will be addressed later in Sections 3.7 and 3.8.

In Figure 5(b), the variation of $\theta(x)/\theta_0$ versus x/L is also linear when the cover plate having streamlined leading-edge profile is situated at $X_0/L = 0$ (dashed line). However, the slope and the local momentum thickness are smaller for the streamlined leading edge than those for the sharp leading edge positioned at the same location $X_0/L = 0$. In addition to the different slopes of $\theta(x)/\theta_0$, Figure 5(b) also indicates that the local momentum thickness across the cavity decreases as the leading edge moves from $X_0/L = 0$ to $X_0/L = 2{\cdot}0$. Large slope of $\theta(x)/\theta_0$ distribution implies higher spreading rate of the shear layer across the cavity mouth. Large momentum thickness of the shear layer is a result of large fluid entrainment across the shear layer (namely, from the high-speed to low-speed side). As a result, the shear layer will roll-up into a matured vortex structure at an early x/L location [Figure 2(b)]. However, in Figure 2(a, c, d), only wavy structures are observed across the cavity mouth because of a small spreading rate and small fluid entrainment.

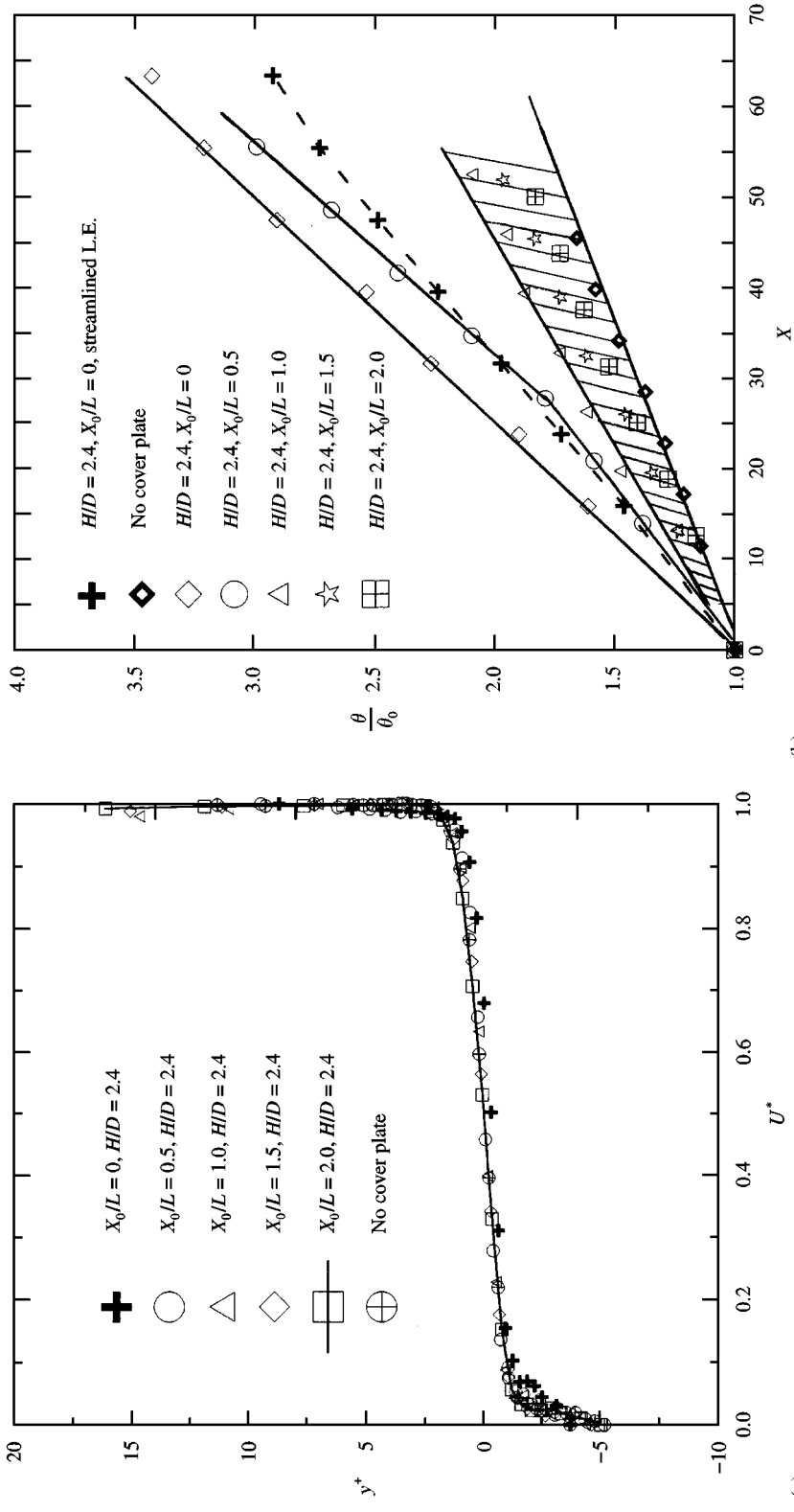

Figure 5(a). Nondimensional mean streamwise velocity profile U^* across the shear layer for various leading-edge locations of the cover plate. The solid line represents the theoretical tanh-velocity profile. Maximum deviation is estimated to be about 3·2% from the theoretical curve. All the velocity profiles are measured at $x/L = 0{\cdot}5$. (b) Streamwise distributions of the local momentum thickness as functions of the distance across the cavity mouth while the leading edge of the cover plate is placed at different X_0/L locations. Both coordinates are normalized by the individual value of the momentum thickness measured at $x = 0$ for different X_0/L locations. The case without cover plate has maximum deviation, about 4·2%.

3.4. Oscillatory Flow Structure

The power spectral density (PSD) distribution of $\tilde{u}(y)$ is defined as $S_u(f) = (\overline{\tilde{u}^2(f)})/\mathrm{d}f$. Figure 6(a–d) shows the PSD distributions of $\tilde{u}(y)$, measured at three different locations along $y = 0$, for the cases without and with a cover plate located at various X_0/L locations. Upstream of $x/L = 0{\cdot}8$ in Figure 6(a), the PSD distributions exhibit only wide-band characteristics at the noise level without any spectral peak. At $x/L = 0{\cdot}8$ of Figure 6(a), a small but discrete peak slightly above the noise level clearly indicates the onset stage of oscillation near the downstream edge shown in Figure 2(a). The peak frequency f_0 corresponds to the most unstable oscillating mode of the shear layer instability. The Strouhal numbers based upon the momentum thickness and the cavity width are $\mathrm{St}_\theta = 0{\cdot}0157 \pm 0{\cdot}0007$ and $\mathrm{St}_L = 0{\cdot}89 \pm 0{\cdot}02$, respectively.

In Figure 6(b), however, dominant peaks are found at nearly the same frequency f_0 with magnitudes well above the noise level when the leading edge of the cover plate is situated above the cavity at $X_0/L = 0$ and $H/D = 2{\cdot}4$. Evidently, the oscillating amplitude is greatly promoted at the early stage ($x/L = 0{\cdot}2$) of the separated shear layer when the leading edge of the cover plate is located at $X_0/L = 0$. However, in Figure 6(b–d), the peak amplitude at $x/L = 0{\cdot}2$ reduces as the leading-edge location of the cover plate moves from $X_0/L = 0$ to $2{\cdot}0$ at the same height. In Figure 6(d), the PSD distribution at $x/L = 0{\cdot}2$ shows a wide band distribution, and the magnitude of the spectral peak is only slightly above the noise level. Significant reduction of the spectral peak amplitude across the cavity in Figure 6(b–d) coincides well with the flow patterns in Figure 2(b–d). Besides, the frequency of each spectral peak remains nearly unchanged (e.g., $f_0 = 3{\cdot}6 \sim 4{\cdot}0 \pm 0{\cdot}03$ Hz). In Figure 6(b), there also exists another smaller peak centred at the first harmonic frequency ($2f_0$) that initiates and prevails downstream of $x/L = 0{\cdot}5$. In Figure 6(b–d), the amplitudes of the spectral peak at the first harmonic frequency ($2f_0$) decrease with those at fundamental frequency (f_0). This is a clear indication to show that the first harmonic component is a result of nonlinear interaction of the fundamental component.

On the other hand, the PSD distributions of $\tilde{u}(y)$ measured at $x/L = 0{\cdot}5$ and $y = 0$ are shown for the sharp [Figure 7(a)] and the streamlined [Figure 7(b)] leading-edge profiles. For both profiles, all the PSD distributions have a dominant spectral peak with magnitudes well above the noise level. The peak frequencies are found to vary slightly from the 4·0 to 3·6 Hz when the leading edge of the cover plate moves from $X_0/L = 0$ to $2{\cdot}0$. The variations of the spectral peak amplitude in Figure 7 and the underlying flow physics will be discussed in Section 3.8.

The Strouhal number, St_θ, defines the nondimensional frequency of the shear layer instability at initial formation stage. When the leading-edge position moves from $X_0/L = 0$ to $2{\cdot}0$ but at a fixed height ($H/D = 2{\cdot}4$), all the St_{θ_0} in Table 1 vary from 0·0132 to 0·0157. These Strouhal numbers are close to the most unstable frequency of shear layer instability ($\mathrm{St}_{\theta_0} = 0{\cdot}017$) predicted by the linear stability theory. For a rectangular cavity (Knisely & Rockwell 1982), the mode II oscillation (or $\lambda = L/2$) also had Strouhal numbers in the range $0{\cdot}0115 < \mathrm{St}_{\theta_0} < 0{\cdot}0226$. Besides, in the present study, the shape factors measured at the upstream edge of the cavity vary in the range $\delta_0^*/\theta_0 = 2{\cdot}28$–$2{\cdot}52 \pm 0{\cdot}12$. This result indicates that the velocity profiles are only slightly blunt (i.e., reduction of θ_0) in the boundary layer at $x = 0$ and do not significantly change its shape. Thus, the initial instability characteristics of the separated shear layer will not be altered significantly because of slight change in the velocity profiles.

When the growing shear layer or vortex impinges on the downstream edge of the cavity, the alternate inward and outward fluid motion, caused by various types of vortex downstream-edge interaction, will generate a disturbance near the downstream edge. This

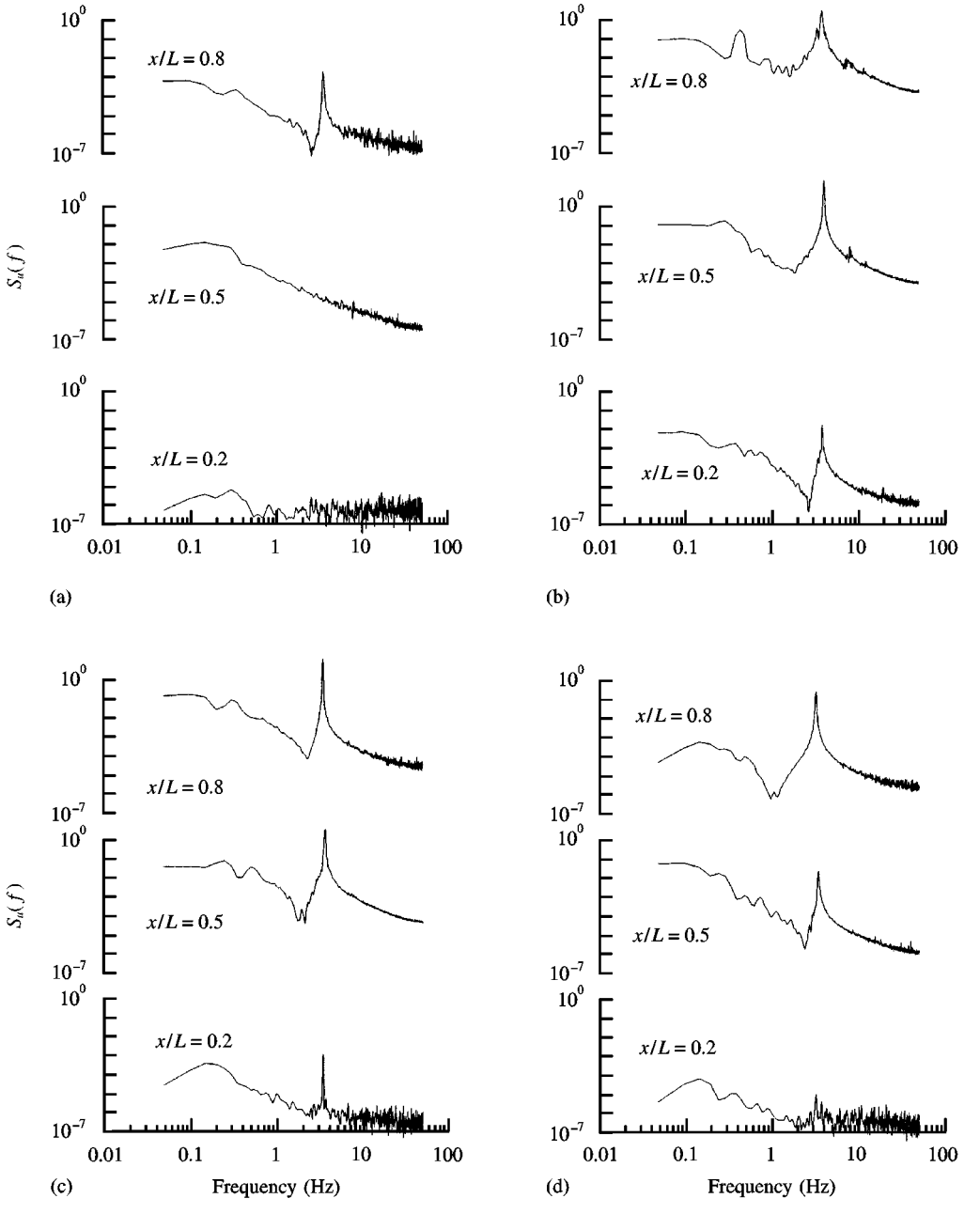

Figure 6. Velocity spectral density measured across the cavity mouth along $y = 0$ for (a) no cover plate, and (b, c, d) with the sharp leading edge of the cover plate, positioned at (b) $X_0/L = 0$ (c) $X_0/L = 1{\cdot}0$ and (d) $X_0/L = 2{\cdot}0$, all for $H/D = 2{\cdot}4$. The spectral peak frequency varies from 3·6 to 4·0 Hz with 0·3% deviation about the central frequency.

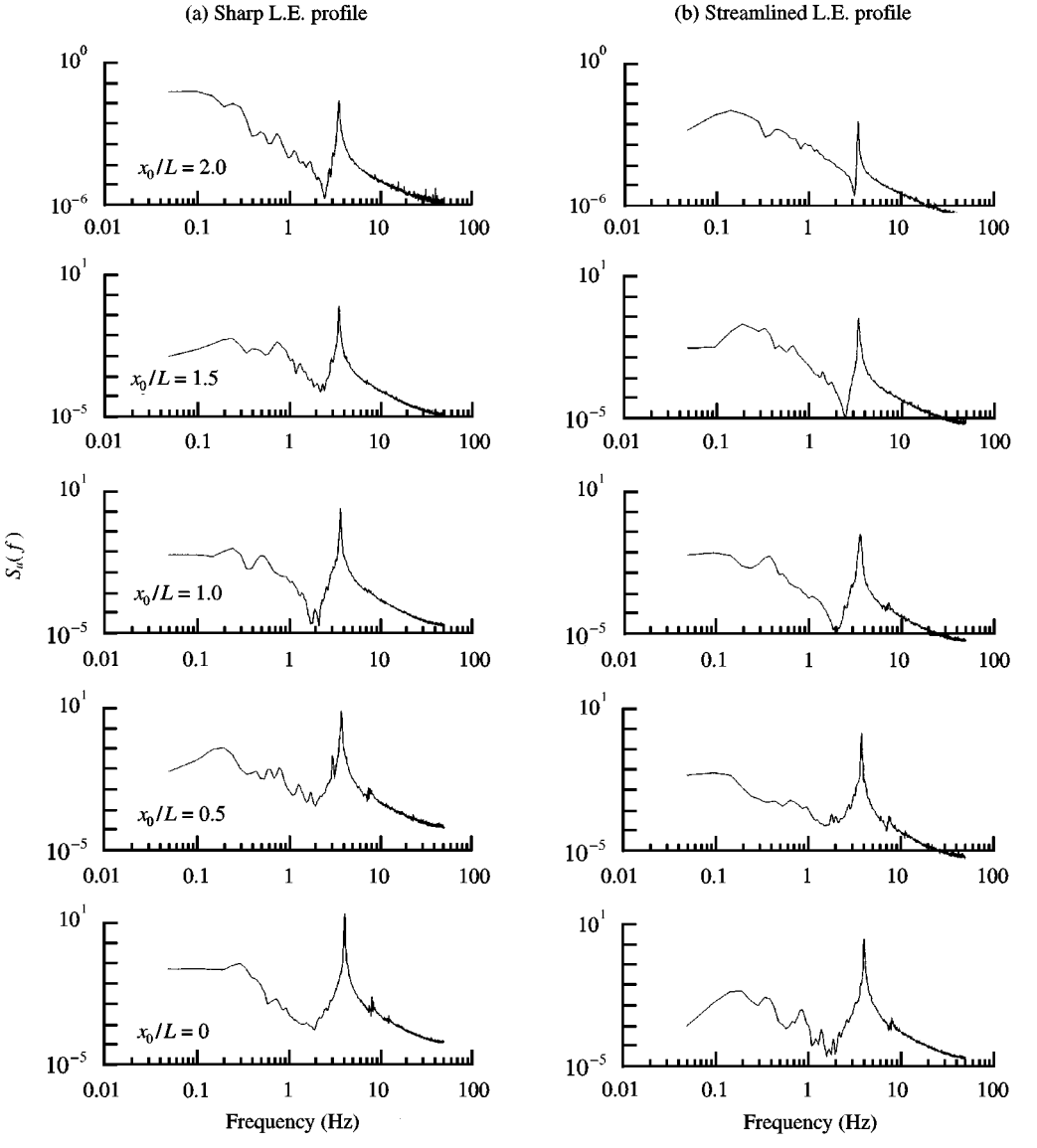

Figure 7. Comparison of the velocity spectra between the (a) sharp and (b) streamlined leading-edge profiles while the leading edge of the cover plate is positioned from $X_0/L = 0$ to 2·0. All velocity spectral densities are measured at $x/L = 0{\cdot}5$ and $y = 0$.

disturbance will create an alternate pressure fluctuation near the downstream edge, and meanwhile propagate to the upstream edge of the cavity. The upstream propagating pressure fluctuation (or feedback) will produce vorticity fluctuation near the upstream edge of the cavity and perturb the separated shear layer. A self-sustained oscillation will occur only when the phase between the feedback and the initial disturbance of shear layer instability (at $x = 0$) differs by $2n\pi - \pi/2$. Here n represents any integer. In alternative form, this phase difference can be expressed as equation (2) (Blake 1980) that has considerable experimental support.

$$\mathrm{St}_L = \frac{U_c}{U_\infty}\left(n - \frac{1}{4}\right), \quad n = 1, 2, 3, \ldots \tag{2}$$

The Strouhal number St_L indicates the wave number across the cavity mouth. In the present study, the convection velocities U_c are estimated to be about 0·52–0·565 U_∞ from the flow visualization videotape (Huang 1998). By substituting the estimated U_c and $n = 2$ into equation (2), the variations of St_L are shown as the solid symbols in Figure 8. On the other hand, the Strouhal numbers, evaluated directly by $\mathrm{St}_L = f_0 L/(U_0)_\infty$ based on the spectral peak frequency f_0 in Figures 6 and 7, are also depicted as open symbols in Figure 8 for various leading-edge locations (X_0/L) and different leading-edge profiles of the cover plate. Thus, the agreement of Struohal numbers in Figure 8 lends further support to the assertion

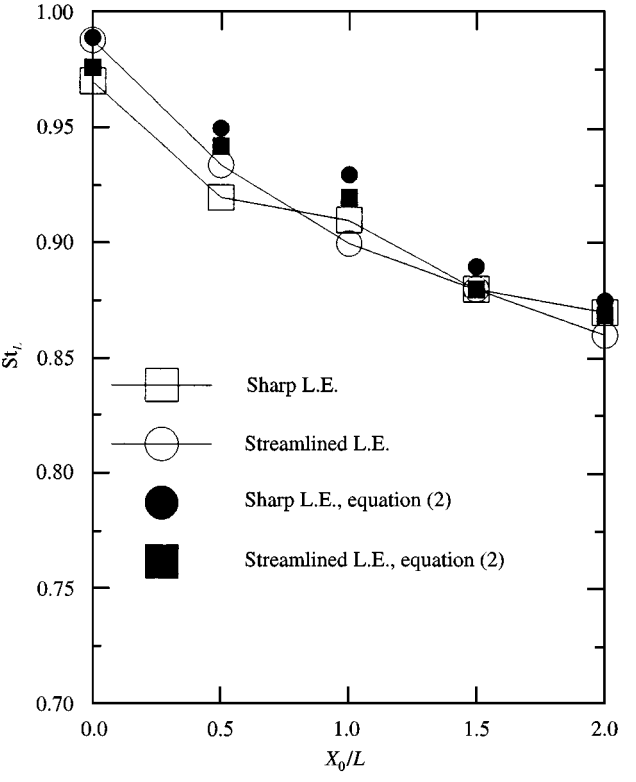

Figure 8. Strouhal number corresponding to the most unstable mode of shear layer instability as a function of the leading-edge locations of the cover plate for either sharp or streamlined leading-edge profiles. The maximum deviation is about 0·6%. The solid symbols are evaluated from equation (2). The open symbols are obtained by the definition $\mathrm{St}_L = f_0 L/(U_0)_\infty$.

that the self-sustained oscillation at fundamental frequency f_0 corresponds to mode II oscillation of shear layer instability within the cavity.

3.5. Streamwise Growth of Oscillation Amplitude

At each x/L location along the cavity mouth, the maximum r.m.s. amplitude of $\tilde{u}(y)$ occurs at an elevation where the local velocity reaches 90% of U_{max}. This elevation is approximately at $y = 0$–2 mm, locates on the high-speed side of the shear layer. The r.m.s. amplitudes of the self-sustained oscillation are extracted from the background noise by the following equation, using a bandwidth of 0·5 Hz about the central frequency ($f_0 = 3{\cdot}6$–$4{\cdot}0$ Hz). Namely,

$$[\overline{(u'^2(f_0))}]^{1/2} = \left[\int_{fl}^{fu} S_u(f)\,\mathrm{d}f\right]^{1/2}. \tag{3}$$

In equation (3), $f_l = f_0 - \Delta f_b/2, f_u = f_0 + \Delta f_b/2$, and Δf_b represents the bandwidth centred at the fundamental frequency (f_0) within which the magnitude exceeds half power of the spectral peak.

In Figure 9, the nondimensional maximum r.m.s. amplitude at frequency f_0 is defined as $u^*_{\text{r.m.s.}} = \text{Maximum}(\tilde{u}_{\text{r.m.s.}})/U_\infty$. All the curves in Figure 9 reveal the streamwise growth of $u^*_{\text{r.m.s.}}$ across the cavity when the cover plate has different leading-edge profiles and is located at various leading-edge locations (X_0/L). In Figure 9, the ordinate scale is logarithmic and the abscissa scale is linear. Therefore, the slope of each curve can be interpreted as the growth (or amplification) rate of the most unstable oscillating mode of shear layer instability. Within the region $x/L < 0{\cdot}1$ where the shear layer oscillation does not begin, the spectral peaks fall below the noise level and the values of $u^*_{\text{r.m.s.}}$ suffer from large uncertainty. Consequently, no reliable data points are available within this region.

In the region $0{\cdot}1 < x/L < 0{\cdot}6$, the magnitudes of $u^*_{\text{r.m.s.}}$ in Figure 9 increase with increasing x/L and reach an individual maximum value at different x/L locations. Within the region $0{\cdot}6 < x/L < 1{\cdot}0$, the amplitude saturation and subsequent decrease in $u^*_{\text{r.m.s.}}$ at the fundamental frequency f_0 are accompanied by the appearance of the first harmonic component ($2f_0$). Formation and growth of the first harmonic component are primarily due to nonlinear interaction of the oscillation at the fundamental frequency (Chang 1996). Further decrease in the magnitude of $u^*_{\text{r.m.s.}}$ at $x/L = 1{\cdot}0$ is caused primarily by the impingement of the shear layer (or a matured vortex) on the downstream edge.

Furthermore, in the region $0{\cdot}1 < x/L < 0{\cdot}6$, the magnitude of $u^*_{\text{r.m.s.}}$ increases when the leading-edge location of the cover plate moves from $X_0/L = 2{\cdot}0$ to 0. These results coincide well with the qualitative flow patterns in Figure 2(a–d). The slope of each curve in Figure 9 shows almost linear variation within the initial growing region (e.g., $x/L = 0{\cdot}1$–$0{\cdot}3$). The largest slope is found to be the case of $X_0/L = 0$. However, the slope decreases as the leading edge of the cover plate moves from $X_0/L = 0$ to 2·0. This clearly indicates that the initial evolution of $u^*_{\text{r.m.s.}}$ obeys a linear stability theory and shows an exponential growth in the streamwise direction. Similar streamwise evolution of $u^*_{\text{r.m.s.}}$ can also be found in Figure 9 when the cover plate of the streamlined leading edge is located at $X_0/L = 0$. However, the amplitude of $u^*_{\text{r.m.s.}}$ for the sharp leading-edge profile is about three or four times higher than that for the streamlined one.

Based on linear stability theory for the tanh-velocity profile, the spatial amplification rate α_i is inversely proportional to the momentum thickness θ_0. Small value of θ_0 implies large amplification rate (or the sensitivity) of the shear layer instability. When the leading edge of the cover plate is positioned at $X_0/L = 0$, significant flow acceleration near the most

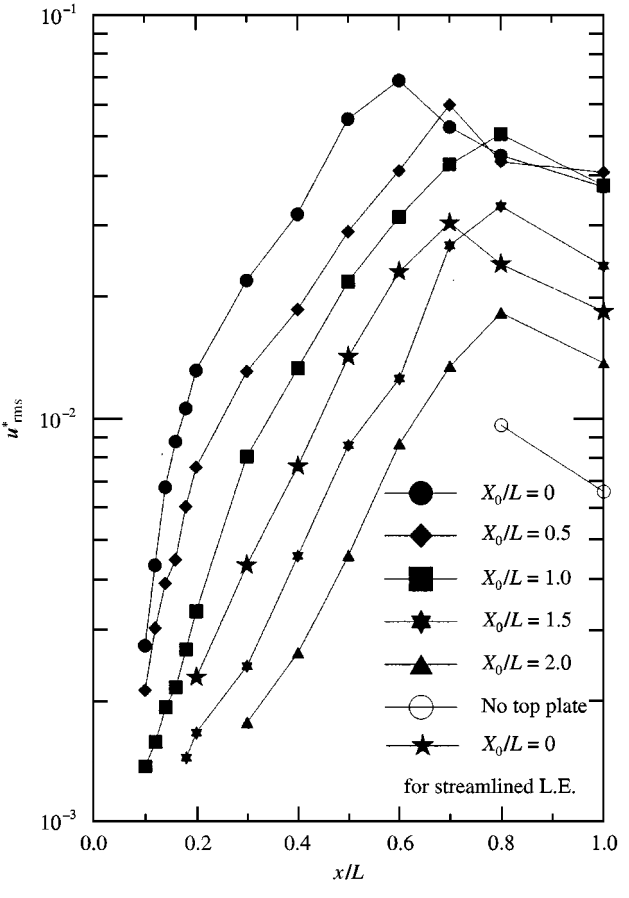

Figure 9. Streamwise variations of the nondimensional maximum r.m.s. amplitude of the most unstable oscillation for different leading-edge profiles and leading-edge locations of the cover plate. All the measurement are taken along the shear layer where the magnitude of the streamwise velocity reaches 90% of the local maximum velocity U_{max}.

sensitive region of the cavity shear layer reduces the local momentum thickness θ_0 by about 15% for sharp leading edge, and about 12% for streamlined leading edge (Table 1). In Table 1, the momentum thickness θ_0 for both leading-edge profiles increases when the leading edge of the cover plate moves from $X_0/L = 0$ to $X_0/L = 2{\cdot}0$. The increasing slope of each curve in Figure 9 correlates well with the decreasing momentum thickness θ_0 in Table 1. This result implies that the flow acceleration near $x = 0$ increases the amplification rate (or sensitivity) of the shear layer instability.

3.6. Boundary Layer Structure and Its Spectrum

When the leading edge of the cover plate is located at $X_0/L = 0$ and $H/D = 2{\cdot}4$, the contours of the mean streamwise velocity $\bar{u}$ for different leading-edge profiles are plotted in Figure 10(a, b). It is intended to illustrate the boundary-layer flow structure near the leading-edge region of the cover plate. The ordinate y_b denotes the distance away from the flat surface of the cover plate and thus $y_b = 0$ represents the location on the flat surface. Evidently, the outer flows are uniform before entering the left boundary in Figure 10(a) and (b). In Figure 10(a), the maximum positive velocity near $x/L = 0{\cdot}3$ and $y_b = 6$ mm implies

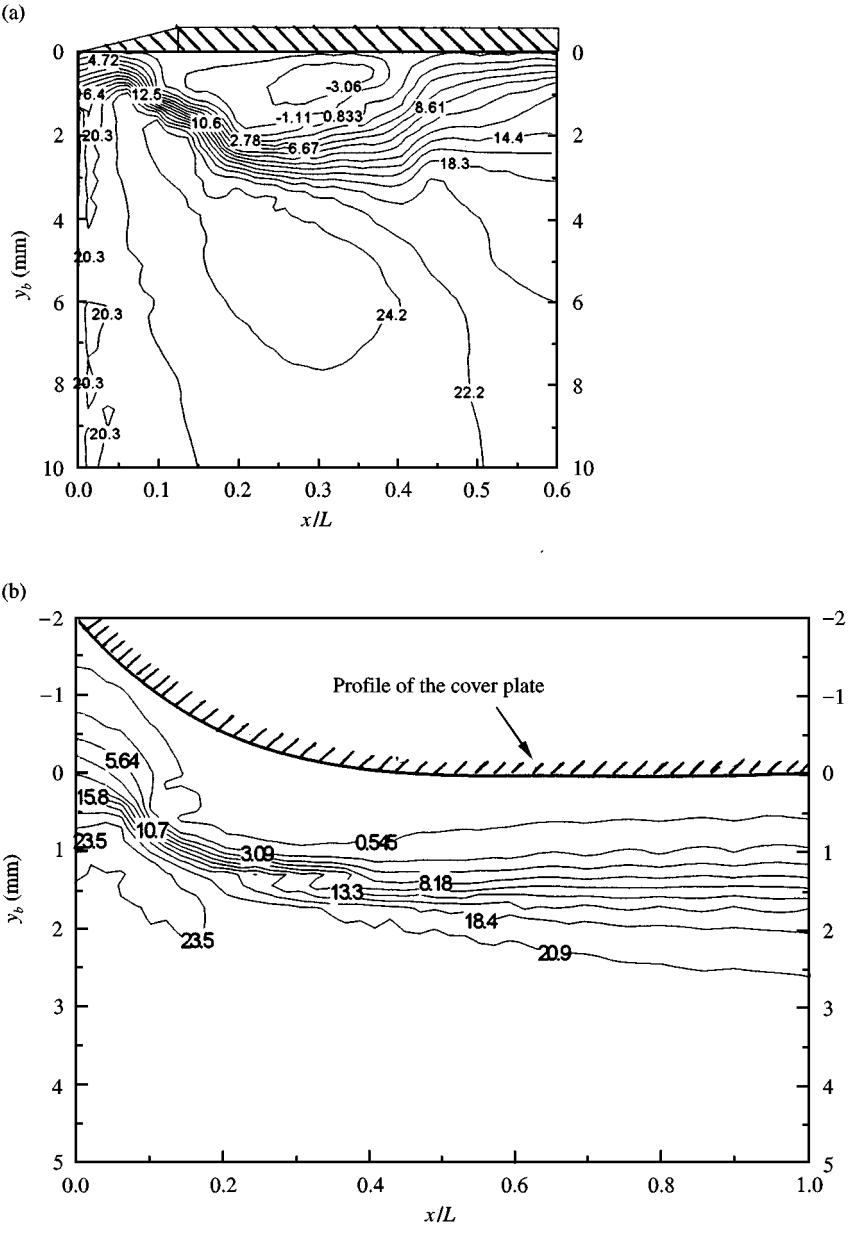

Figure 10. Contours of the mean streamwise velocity showing the boundary-layer structure near the leading-edge regime of the cover plate with (a) sharp leading-edge profile, and (b) streamlined leading-edge profiles. In both cases, the leading edge is located at $X_0/L = 0$ and $H/D = 2{\cdot}4$ above the cavity. The thickness of the cover plate is 5 mm.

that the outer flow accelerates within the region $x/L < 0{\cdot}3$ and then slightly decelerates in the region downstream of $x/L = 0{\cdot}3$. This flow acceleration characteristic is similar to those illustrated in Figure 4. However, there exists a region of dense contours that represents the shear layer due to flow separation from the surface of the cover plate. Furthermore, in the region closely adjacent to the cover plate ($y_b < 2$ mm), there appears a region of negative velocity, extending from $x/L = 0{\cdot}1$ to $0{\cdot}45$. Downstream of $x/L = 0{\cdot}45$, the mean flow is reattached to the surface of the cover plate. This clearly indicates the footprint of a recirculation region. However, for the cover plate having streamlined leading edge located at $X_0/L = 0$, the contours of $\bar{u}$ in Figure 10(b) show that the boundary-layer flow remains attached to the surface of the cover plate within $0 \leq x/L \leq 1{\cdot}0$. Additional velocity measurements within $0 \leq x/L \leq 3{\cdot}0$ for the streamlined leading-edge profile clearly indicate that the attached flow extends farther downstream of the cavity mouth without any signature of flow separation (Huang 1998).

To reveal the frequency components either in the recirculation region [Figure 10(a)] or in the attached boundary-layer flow [Figure 10(b)], the PSD distributions of $\tilde{u}(y)$ measured at various transverse locations across the boundary layer are shown in Figure 11(a, b). At $y_b = 2{\cdot}8$ mm of Figure 11(a), the PSD distributions exhibit a dominant peak at $f_{sp} = 19$ Hz, which corresponds to the shear layer instability separated from the surface of the cover plate. The magnitude of the spectral peak at f_{sp} decreases as the measuring location moves close to the cover plate. In Figure 11(b), however, there is no evidence to show the existence of the frequency component f_{sp}, because the boundary-layer flow is attached to the surface. When the PSD distributions of $\tilde{u}(y)$ in Figure 11(a) and 11(b) are compared, the fluctuating amplitudes within the low-frequency band (between the arrows) are mainly contributed by the existence of a recirculation region closely adjacent to the cover plate. This low-frequency band has a Strouhal number $\mathrm{St}_L = 0{\cdot}025$–$2{\cdot}5$ that contains the self-sustained oscillating frequency of mode II ($\mathrm{St}_L = 0{\cdot}86$–$0{\cdot}98$).

Besides, the fluctuating amplitudes of the PSD distributions are smaller in Figure 11(b) than those in Figure 11(a) by at least three orders of magnitude. Significant differences in the fluctuating amplitude can also be referred to the typical velocity time signals shown on the top of each column. However, the magnitudes of $u^*_{\mathrm{r.m.s.}}$ in Figure 9 for different leading-edge profiles do not change proportionally to this significantly different fluctuating level (Figure 11). This clearly indicates that the boundary-layer structure (both the fluctuating amplitude and frequency band) adjacent to the cover plate is only one of the important mechanisms to affect the shear layer instability across the cavity.

3.7. Shear Layer or Vortex and Downstream Edge Interaction

When the shear layer or vortex impinges on the downstream edge of the cavity, the alternate inward and outward fluid motion, caused by various types of vortex downstream-edge interaction, will generate a disturbance near the downstream edge. This disturbance will create an alternate pressure fluctuation near the downstream edge, and meanwhile propagate to the upstream edge of the cavity to perturb the separated shear layer. The agreement in Strouhal numbers in Figure 8 further ensure the phase condition between the feedback and the initial disturbance of shear layer instability (at $x = 0$) to maintain the self-sustained oscillation. In addition to the phase condition, the oscillating amplitude within the cavity is also closely related to the strength of the feedback.

As the shear layer (or vortex) encounters the downstream edge of the cavity, four possible events of shear layer (or vortex) and downstream edge interaction can be found in cavity flows (Knisely & Rockwell 1982). These events are caused by the impingement of the shear layer (or vortex) on different elevations of the downstream surface. Classifications of the

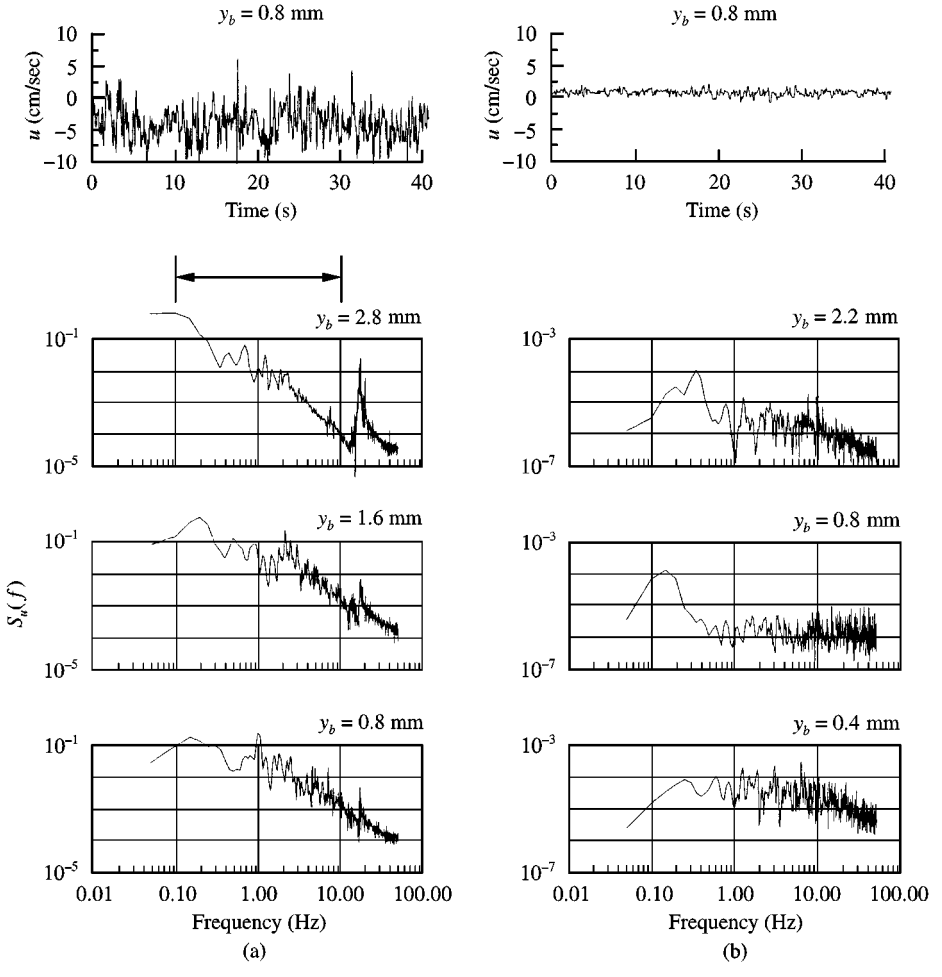

Figure 11. Power spectral densities across the boundary layer of the cover plate showing the fluctuating level and the frequency of the flow instability measured at $x/L = 0{\cdot}3$ for (a) sharp and (b) the streamlined leading-edge profiles. Note that the scale ranges of the ordinates in (a) are at least two orders of magnitude higher than those in (b). Typical velocity time signals are shown on the top of each column.

interaction type are demonstrated in Figure 12. When the wavy pattern is observed in the cavity [Figure 2(a, c, d)], the height between the wave trough and the wavefront is defined as Δ. The height of the wavefront above the downstream edge ($y = 0$) is denoted by h. However, the vortex size is defined as Δ and the height of the vortex top above the downstream edge is denoted by h if a matured vortex is formed near the downstream edge [Figure 2(b)]. For $h \geq \Delta$, the interaction is called one of the complete escape type (CE). If $\Delta/2 < h < \Delta$, the type of interaction is denoted as one of partial escape (PE). When $\Delta/4 < h < \Delta/2$, an interaction type of partial clip (PC) is defined; if $0 \leq h \leq \Delta/4$, it is called the complete clip type (CC). Types of shear layer (or vortex) and downstream edge interaction are acquired over 570 oscillating cycles from the recorded flow visualization.

As shown in Figure 13, the probabilities of the CC (30%) and PC (44%) type interaction are the highest when the cover plate is positioned above the cavity at $X_0/L = 0$ and $H/D = 2{\cdot}4$. The probabilities of CC and PC type interaction decrease as the leading-edge location moves from $X_0/L = 0$ to $2{\cdot}0$. On the contrary, the probabilities of the CE and PE

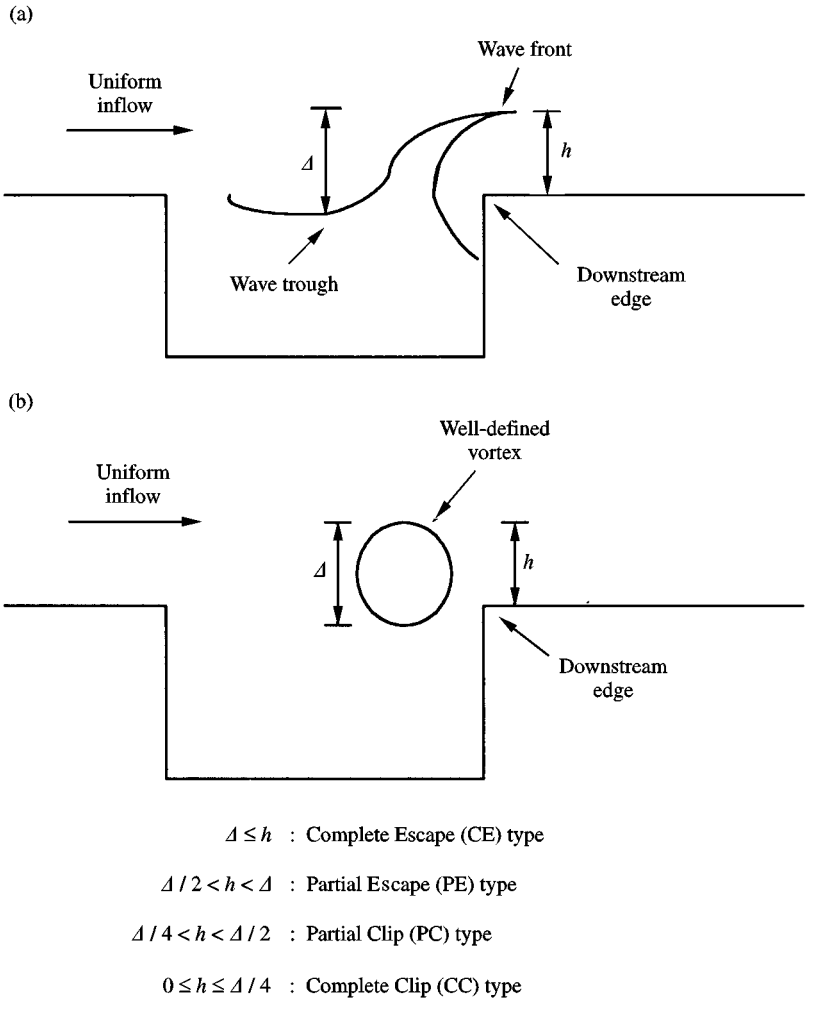

Figure 12. Demonstrations of (a) the shear layer/downstream edge interaction, (b) the vortex/downstream-edge interaction.

type interaction increase as the leading edge of the cover plate moves from $X_0/L = 0$ to 2·0. Based on the long-time observation, though qualitatively, increasing probabilities of CC and PC type interaction imply that the shear layer is further deflected into the cavity. When the leading edge is situated within the region $0 \leq X_0/L < 1{\cdot}0$, the inward-deflected shear layer is caused primarily by the growth of boundary layer adjacent to the cover plate. However, as the leading edge is located within $X_0/L \geq 1{\cdot}0$, the inward-deflected shear layer is caused by the slightly higher speed induced by flow acceleration occurring downstream of the cavity (Figure 4). For the streamlined leading-edge profile located at $X_0/L = 0$, the probabilities of CC and PC type interactions are lower than for the sharp leading edge because of the thinner boundary layer thickness adjacent to the cover plate.

The reduction in the slope of $\theta(x)$ distribution [Figure 5(b)] and the increase in the local momentum thickness θ_0 (Table 1) correlate well with the decreasing probabilities of CC and PC type interaction [Figure (13)] when the leading edge of the cover plate moves from $X_0/L = 0$ to 2·0. This correlation further ensures that insertion of the horizontal cover plate

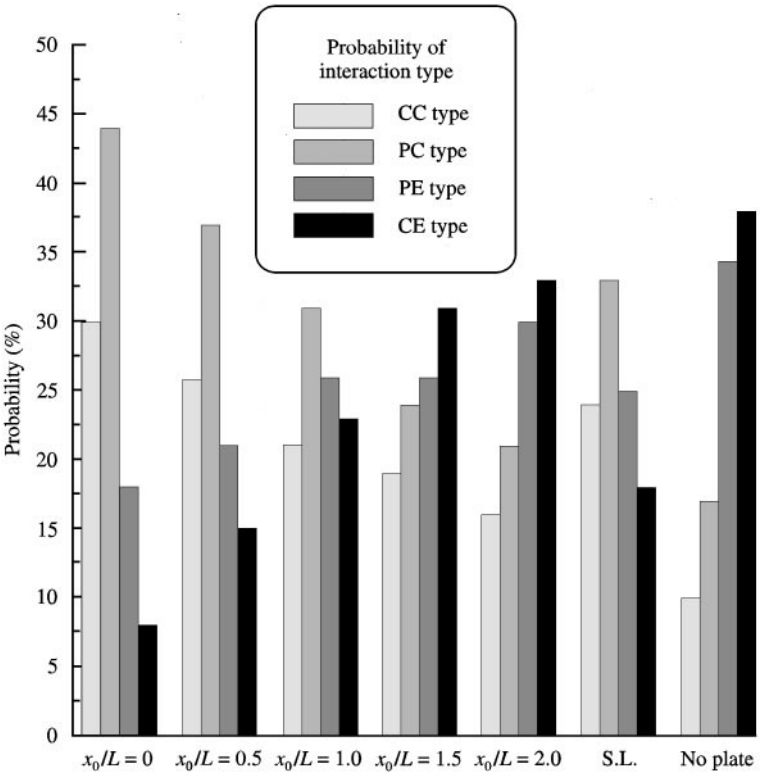

Figure 13. Probabilities of four types of shear layer (or vortex) and downstream edge interaction for different leading-edge profiles and for various leading-edge locations of the cover plate. SL represents the case of streamlined leading-edge profile.

above the cavity will deflect the shear layer into the cavity. The higher the probabilities of CC and PC type interaction, the further is the shear layer deflected into the cavity. The magnitude of feedback disturbance depends on the impingement location on the downstream face. Thus, impingement of the further inward-deflected shear layer on the downstream edge of the cavity will generate large amplitudes of fluctuating pressure and lead to stronger feedback.

3.8. Mechanisms Leading to Enhanced Oscillation

The mechanisms for the enhanced oscillating amplitude within the cavity can be demonstrated in Figure 14. The perturbations come mainly from three sources. First of all, insertion of the horizontal cover plate does impose a favourable streamwise pressure gradient at a different region across the cavity mouth (Figure 4). The flow acceleration, associated with this favourable pressure gradient, will increase the amplification rate of the shear layer instability. Second, the frequency components and velocity fluctuating level in the boundary layer adjacent to the cover plate give another opportunity to modify the shear layer instability. The modification can be effective as long as the fluctuating amplitude in the boundary-layer structure of the cover plate is higher than the threshold value. Third, the separated shear layer is deflected into the cavity leading to higher probabilities of CC and PC interaction types. Higher probabilities of CC and PC interaction will cause stronger feedback. Then, stronger feedback will synchronously amplify the initial disturbance of the

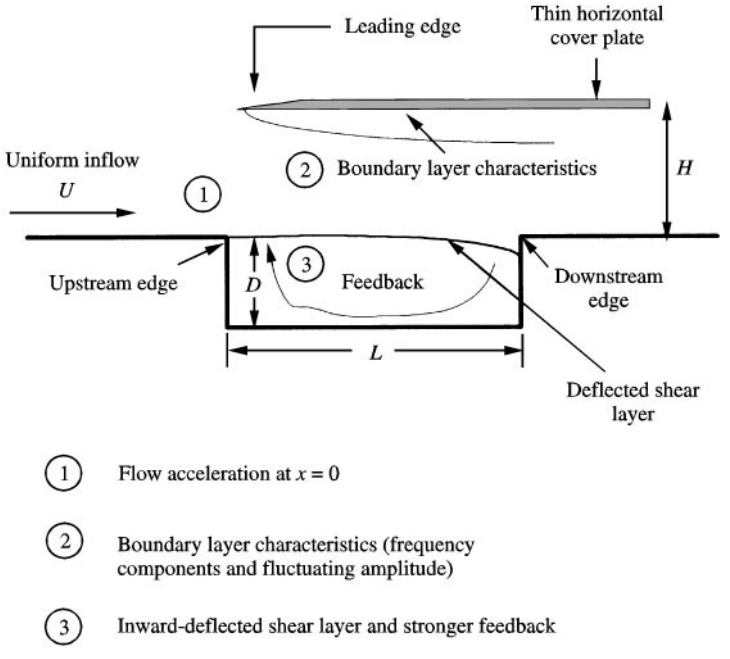

Figure 14. Pictorial illustration of the mechanism leading to the enhanced self-sustained oscillation within the cavity.

more sensitive shear layer (due to reducing θ_0) and enhance the oscillating amplitude within the cavity.

In the present study, the enhancement of the self-sustained oscillation within the cavity is more effective when the leading edge of the cover plate is positioned at $X_0/L < 1{\cdot}0$. However, the enhancement decreases significantly as the leading edge of the cover plate moves to the downstream locations (e.g., $X_0/L \geq 1{\cdot}0$). In the former situations, all three mechanisms are equally important for the promoted self-sustained oscillation. However, in the latter situations, the flow acceleration and the boundary-layer induction are negligible. Thus, the inward-deflected shear layer will result in stronger feedback and becomes the major mechanism to induce large oscillating amplitude within the cavity. In other words, when the leading edge of the cover plate is located within the region $X_0/L \geq 1{\cdot}0$, the third effect becomes the important mechanism to enhance the oscillating amplitude within the cavity. The proposed mechanisms in Figure 14 can be further confirmed by the significantly different slopes of $\theta(x)/\theta_0$ distributions in Figure 5(b) when the leading edge is located within the regions $X_0/L < 1$ and $X_0/L \geq 1$, respectively. For the case $X_0/L = 0{\cdot}5$ in Figure 5(b), the smaller slope in the region $x/\theta_0 < 27$ is a result of diminishing flow acceleration near $x = 0$. However, the sudden change of the slope of $\theta(x)/\theta_0$ distributions near $x/\theta_0 \approx 27$ is induced simultaneously by all three mechanisms mentioned above. Furthermore, in Figure 7(a) (sharp leading-edge profile), the spectral peak amplitudes are at least one or two orders of magnitude higher for $X_0/L < 1{\cdot}0$ than for $X_0/L \geq 1{\cdot}0$. Again, the distinct differences in the spectral peak amplitude in Figure 7(a) strongly suggest that the modification mechanisms are quite different when the leading edge is located within the region $X_0/L < 1{\cdot}0$ and $X_0/L \geq 1{\cdot}0$. Similar mechanisms can be applied to the case of streamlined leading-edge profile [Figure 7(b)], except for the smaller peak amplitude.

The differences in the spectral peak amplitudes between the sharp and the streamlined leading-edge profiles may also be discussed based on the proposed mechanism in Figure 14.

In Figure 4, the flow acceleration effect is nearly the same for both leading-edge profiles located at $X_0/L = 0$. As a consequence, when the leading edge of the cover plate is located within the region $X_0/L < 1{\cdot}0$, the second and the third mechanisms are stronger for the sharp leading-edge profile and are mainly responsible for the differences in the spectral peak amplitudes between Figures 7(a) and 7(b). However, when the leading edge of the cover plate is located within the region $X_0/L \geq 1{\cdot}0$, the second effect induced by the boundary-layer structure adjacent to the cover plate becomes minor. Thus, the inward-deflected shear layer becomes the dominant mechanism to modify the shear layer instability. When the leading edge of the cover plate is situated at $X_0/L = 2{\cdot}0$, statistical results (Huang 1998) show that the probabilities of the CC and PC type interaction are slightly higher for the sharp leading-edge profile than for the streamlined one. Correspondingly, the spectral peak amplitude is slightly higher for the sharp leading edge than for the streamlined one [Figure 7(a) and 7(b)] at $X_0/L = 2{\cdot}0$.

At much higher Reynolds number, the flow structure between the cover plate and the cavity, and in the boundary layer of the cover plate will become highly three-dimensional. Therefore, the mechanisms responsible for modifying the shear layer instability at higher Reynolds number may be different.

4. CONCLUSIONS

The oscillatory characteristics of cavity shear layer in the presence of a horizontal cover plate are investigated by way of laser Doppler velocimetry. The Reynolds number based on the momentum thickness at the flow separation point (or the upstream edge of the cavity) is about $\mathrm{Re}_{\theta_0} = 171 \pm 5$. The key mechanisms responsible for this modification have been explored by experiments. When the leading edge of the cover plate is located right above the most sensitive region of the shear layer, the oscillating amplitude within the cavity is enhanced most effectively. However, the effectiveness decreases significantly as the leading edge of the cover plate moves downstream of the cavity. Three mechanisms are found to possibly perturb the shear layer instability across the cavity. First of all, insertion of a horizontal cover plate does impose a favourable streamwise pressure gradient across the cavity mouth. The associated flow acceleration increases the amplification rate of the shear layer instability and makes the shear layer more sensitive to external perturbations. Secondly, the frequency components and the velocity fluctuation level in the boundary layer adjacent to the cover plate also provide another opportunity to modify the shear layer instability. Third, higher probabilities of PC and CC types of shear layer (or vortex) and downstream edge interaction clearly indicates that the shear layer is further deflected into the cavity, resulting in stronger feedback. In the cases $X_0/L < 1{\cdot}0$, the flow acceleration, the boundary-layer flow structure adjacent to the cover plate and the stronger feedback due to the inward-deflected shear layer are equally important factors to enhance the oscillating amplitude within the cavity. For cases with $X_0/L \geq 1{\cdot}0$, the first and the second effects become diminished and the stronger feedback due to the inward-deflected shear layer becomes the important factor. The mechanism proposed here may change for different ranges of Reynolds number and other geometric alterations, and they deserve further investigations.

ACKNOWLEDGEMENTS

The authors are grateful for the project supported by the National Science Foundation of the Republic of China under the grant no. NSC-87-2212-E-005-026.

References

Blake, W. K. 1980 *Mechanics of Flow-Induced Sound and Vibration*, Vol. 1: *General Concepts and Elementary Sources*, Chapter 3. London: Academic Press, Inc.

Chang, C. W. 1996 Investigation on the oscillatory characteristics of shear layer over cavity with horizontal top plate. Master Thesis, Department of Mechanical Engineering, National Chung Hsing University, Taichung 40227, Taiwan, R. O. C.

DeMetz, F. C. & Farabee, T. M. 1977 Laminar and turbulent shear flow induced cavity resonance. AIAA Paper 77–1293.

Ethembabaoglu, S. 1973 On the fluctuating flow characteristics in the vicinity of gate slots. Ph.D. Dissertation, Division of Hydraulic Engineering, University of Trondheim, Norwegian Institute of Technology, Trondheim, Norway.

Franke, M. E. & Carr, D. L. 1975 Effect of geometry on open cavity flow-induced pressure oscillations. AIAA Paper 75–492.

Ghaddar, N. K., Korczak, K. Z., Mikic, B. B. & Patera, A. T. 1986 Numerical investigation of incompressible flow in grooved channels; Stability and self-sustained oscillation. *Journal of Fluid Mechanics* **163,** 99–127.

Gharib, M. 1987 Response of the cavity shear layer oscillations to external forcing. *AIAA Journal* **25,** 43–47.

Gharib, M. & Roshko, A. 1987 The effect of flow oscillations on cavity drag. *Journal of Fluid Mechanics* **177,** 501–530.

Heller, H. H. & Bliss, D. 1975 The physical mechanism of flow-induced pressure fluctuations in cavities and concepts for their suppression. AIAA Paper 75–491.

Huang, S. H. 1998 Experimental study and control on oscillatory characteristics of cavity shear layer. Master Thesis, Department of Mechanical Engineering, National Chung Hsing University, Taichung 40227, Taiwan, R. O. C.

Knisely, C. & Rockwell, D. 1982 Self-sustained low frequency components in an impinging shear layer. *Journal of Fluid Mechanics* **116,** 157–186.

Michalke, A. 1972 The instability of free shear layers. *Progress in Aeroscience* **12,** 213–239.

Miksad, R. W. 1972 Experiments on non-linear stages of free shear layer transition. *Journal of Fluid Mechanics* **56,** 695–719.

Pereira, J. C. F. & Sousa, J. M. M. 1995 Numerical investigation of flow oscillations in a rectangular cavity. *ASME Journal of Fluids Engineering* **117,** 68–74.

Rockwell, D. 1983 Oscillations of impinging shear layer. *AIAA Journal* **21,** 645–664.

Rockwell, D. & Naudascher, E. 1978 Review of self sustaining oscillations of flow past cavities. *ASME Journal of Fluids Engineering* **100,** 152–165.

Rockwell, D. & Knisely, C. 1979 The organized nature of flow impingement upon a corner. *Journal of Fluid Mechanics* **93,** 413–432.

Vakili, A. D., Cooper, G. C. & Schatt, D. E. 1993 Effect of upstream injection patterns on cavity flow aero-acoustics. In *Experimental Heat Transfer, Fluid Mechanics and Theromodynamics*, Vol. 2, (eds Kelleher, M. D., Shah, R. K., Sreenivasan, K. R. & Yoshi, Y.), pp. 1157–1164. Amsterdam: Elsevier.

Zaman, K. B. M. Q. & Hussain, A. K. M. F. 1980 Vortex pairing in a circular jet under controlled excitation; Part I. General jet responses. *Journal of Fluid Mechanics*, **101,** 449–491.